frontiers | Frontiers in Materials

TYPE Original Research
PUBLISHED 02 February 2023
DOI 10.3389/fmats.2023.1109890

OPEN ACCESS

EDITED BY
Yanfei Liu,
Beijing Institute of Technology, China

REVIEWED BY
Linmao Qian,
Southwest Jiaotong University, China
Qunfeng Zeng,
Xi'an Jiaotong University, China
Tianyi Sui,
Tianjin University, China

*CORRESPONDENCE
Liran Ma,
maliran@tsinghua.edu.cn

SPECIALTY SECTION
This article was submitted to Colloidal Materials and Interfaces, a section of the journal Frontiers in Materials

RECEIVED 28 November 2022
ACCEPTED 11 January 2023
PUBLISHED 02 February 2023

CITATION
Han K, Ma P, Ma L, Tian Y and Luo J (2023), Investigation of the running-in process in photoinduced superlubricity.
Front. Mater. 10:1109890.
doi: 10.3389/fmats.2023.1109890

Investigation of the running-in process in photoinduced superlubricity

Ke Han, Pingsu Ma, Liran Ma*, Yu Tian and Jianbin Luo

State Key Laboratory of Tribology in Advanced Equipment, Tsinghua University, Beijing, China

Photoinduced superlubricity on TiO_2 surfaces is a newfound phenomenon which draws researchers' attention. This study provides a new method to achieve superlubricity (COF<0.01) with an external light field. However, photoinduced superlubricity can only be realized under specific conditions. Improper running-in conditions, such as speed, load, and pH value, will lead to superlubricity failure even after ultraviolet illumination on the TiO_2 surface. In this paper, different running-in loads, speeds, or pH values were used in the experiment of photoinduced superlubricity, and the worn surfaces after running-in and testing in 70% v/v glycerol aqueous solution were investigated thoroughly. Results reveal that the morphology of worn scars differs under different running-in conditions. While the running-in speeds and loads are too low (<0.03 m/s and <2 N) or too large (>0.1 m/s and >9 N), the photoinduced superlubricity will fail because of wrong lubrication state. When the pH value of running-in solution is less than 4.5, photoinduced superlubricity is easier to achieve. In discuss, mixed lubrication is believed to be the key to success of photoinduced superlubricity, because the elastohydrodynamic effect, doublelayer effect and adsorption of glycerol molecules works at the same time. In addition, due to the formation of the SiO_2 layer on the Si_3N_4 ball and better attraction to lubricant molecules with hydroxyl radicals on the TiO_2 surface, running-in in solutions with low pH values contributes to the success of photoinduced superlubricity. In any event, the ultraviolet illumination can reduce the friction coefficient of the TiO_2/Si_3N_4 tribological system and can realize photoinduced superlubricity under appropriate running-in conditions.

KEYWORDS

running-in, superlubricity, photoinduced superlubricity, glycerol, TiO_2

Introduction

Frictional force was predicted to vanish between two sliding clean solid surfaces theoretically in 1990s (Hirano and Shinjo, 1990). In practice, superlubricity or super-low friction refers to the situation in which the coefficient of friction is less than .01 (Erdemir et al., 2007). In recent years, solid and liquid superlubricity systems have been rapidly developed. Lubrication materials including graphite (Dienwiebel et al., 2005; Vu et al., 2016; Li et al., 2018; Sha et al., 2020), diamond-like carbon (DLC) films (Erdemir et al., 2000; Chen et al., 2014; Liu and Zhang, 2022; Tian et al., 2022), and two-dimensional (2D) materials (such as molybdenum disulfide, graphene, and boron nitride) (Liu et al., 2018a; Yin et al., 2021; Tian et al., 2022; Wu et al., 2022) are verified to achieve solid superlubricity, due to their weak interlayer interaction under specific experimental conditions (Han et al., 2022). Different liquid superlubricity systems have been developed as well, such as biomaterial superlubricity systems (Li et al., 2012; Duan et al., 2019), acid mixed solution-based superlubricity systems (Li et al., 2011; Li et al., 2013a; Li et al., 2013b; Ge et al., 2018a), oil-based superlubricity systems (Li et al., 2015a; Li

et al., 2015b; Liu et al., 2019), and solid additive superlubricity systems (Ge et al., 2018b; Wang et al., 2018; Ge et al., 2019a; Wang and Liu, 2020). Many chemical and physical reactions on the surfaces of contact areas contribute to the superlubricity in these systems, such as the hydration effect, electric double-layer effect, and hydrodynamic effect (Luo et al., 2021; Han et al., 2022).

In most macro-scale tribological experiments between ceramic friction pairs, such as Si_3N_4, glass, and sapphire, a running-in process is often required, which goes through high-friction and friction-decreasing regions to achieve stable liquid superlubricity (Li et al., 2011; Li et al., 2013a; Li et al., 2013b; Li et al., 2015a; Li et al., 2015b; Deng et al., 2016). The high-friction region during the running-in process contributes to most of the wear and significantly reduces the contact pressure (Jia et al., 2019). In addition, the polishing effect during the running-in process helps reduce the roughness of contacting surfaces and the collision among asperities, which can provide favorable conditions for elastohydrodynamic lubrication (Deng et al., 2016). The formation of a tribochemical layer on silicon nitride sliding in water or acid aqueous solution is believed to be another key to achieving superlubricity in systems with silicon nitride friction pairs (Xu and Kato, 2000; Li et al., 2015b; Deng et al., 2016; Ge et al., 2019b; Han et al., 2019). The adsorption of hydrogen ions or hydrated ions on this tribo-induced silica layer generated repulsive double-layer forces or hydration repulsive forces that ensure large load-carrying capacity and finally contribute to achieving superlubricity (Deng et al., 2016; Han et al., 2019). The necessity of the running-in process in superlubricity is undoubted. However, inappropriate conditions during the running-in process still lead to the negative results of achieving superlubricity in most water-based systems. Large load, too low or too high speed, or suboptimal pH value of the solution during the running-in process can all result in superlubricity failure (Li et al., 2014; Xiao et al., 2017; Jiang et al., 2021).

However, liquid superlubricity still needs to be further expanded for research studies and engineering applications. Using an external field to control friction has been studied for years, such as electric field (Goto, 1995; Jiang et al., 2014; de Wijn et al., 2016; Liu et al., 2018b), magnetic field (Zaidi and Senouci, 1999; Hase and Mishina, 2010), light field (Wang et al., 2009; Liu and Broer, 2014; Sasaki et al., 2017; Tang et al., 2020; Perotti et al., 2021; Ma et al., 2022; Tang et al., 2022), and temperature changes (Evoy et al., 2000; Schirmeisen et al., 2006). Controlling friction using the light field is believed to be environmentally friendly, and research studies have been carried out on this. Photosensitive organic materials such as diarylethene (Tang et al., 2020) and azobenzene (Tang et al., 2022) are widely used because their molecular configuration will be changed by an external field, which further influences the lubrication of the tribo-system. TiO_2 is a photosensitive ceramic material that is widely used in photocatalysis because of the emergence of oxygen vacuums and hydroxyl radicals after ultraviolet treatment (Linsebigler et al., 1995; Wang et al., 1999; Nakata and Fujishima, 2012). In addition, tribological researchers have found that photoinduced changes bring about friction variations, due to the interaction between two friction pairs or the water orientations on TiO_2 surfaces (Wang et al., 2009; Perotti et al., 2021; Ma et al., 2022). Our group has found that photoinduced superlubricity can be achieved in the Si_3N_4/TiO_2 tribosystem, and the mechanism is the enhancement of adsorption of lubricant molecules after ultraviolet illumination.

The mixture of acid and glycerol solutions is demonstrated to achieve superlubricity after the ultraviolet treatment under specific running-in conditions. However, the mechanism of photoinduced superlubricity failure on the TiO_2 surface in this system is not clear. In this paper, the influence of the running-in process on the liquid photoinduced superlubricity system is studied. Different topographies and reactions on the worn scar, which arose from the variation of the conditions during the running-in process, are revealed to explain the mechanism of both the success and failure of photoinduced superlubricity.

Materials and methods

Materials

Glycerol used in this experiment had a purity of 99.5%, and sulfuric acid (H_2SO_4) and sodium hydroxide (NaOH) had purity levels over 99.7%. All chemicals were used without further treatment. Pure sulfuric acid and sodium hydroxide samples were diluted with different amounts of deionized water to adjust to special pH values (pH = 1–5 for acid and pH = 9 for hydroxide), and glycerol samples were diluted to 70% volume fractions (with a viscosity of 28 mPa s).

Methods

The friction tests were carried out on a universal micro-tribotester (UMT-5, Bruker) in a rotational mode with a ball-on-disk configuration. The normal and frictional forces were characterized using a two-dimensional force sensor, and the measurement accuracy of the friction coefficient was ±0.001. The ambient temperature was ~25°C and the relative humidity was 20%–40% during the whole experiment. The friction pairs were the Si_3N_4 ball with a diameter of 12 mm and a TiO_2 plate with a surface roughness of 20 nm. Before the test, Si_3N_4 balls and TiO_2 plates were cleaned in acetone and then ethanol *via* sonication for 15 min in each step, followed by washing in pure water and drying at 120°C for 1 h. First, 10–30 μl (according to the rotation radiuses to ensure the same lubricant volume per unit length) sulfuric acid (pH = 1.5) was added dropwise on the TiO_2 surface. During the running-in process, different speeds (0.019–0.283 m/s), rotation radiuses (3 mm, 6 mm, and 9 mm), and loads (1–12 N, corresponding to the average contact pressure of 293 MPa and 670 MPa according to the Hertz contact theory) were set to explore the influence of running-in conditions. After the friction coefficient became stable at the end of the running-in process, the residual sulfuric acid solution was cleaned with deionized water and dried using a rubber suction bulb. As for the UV-treated group, after the running-in process, the surface of TiO_2 was cleaned and treated with UV illumination for 2 h, while no UV treatment was applied on the experiment group (dark). Then, 5 μl 70% v/v glycerol aqueous solution was added dropwise on the worn scar of TiO_2. The speed dependence experiment was carried out by applying high speed to low speed (0.283 m/s to 0.019 m/s) and low speed to high speed.

The topography and curvature radius or contact radius of the friction surface were investigated using the non-contact optical three-dimensional interference profilometer (Nexview, ZYGO Lamda). The chemical elements on the worn surfaces after lubrication were detected using an X-ray photoelectron spectroscope (XPS, PHI Quantera II).

Results

As shown in Figure 1A, after the running-in period in sulfuric acid solution for 300 s, the friction coefficient of the Si_3N_4/TiO_2 tribological

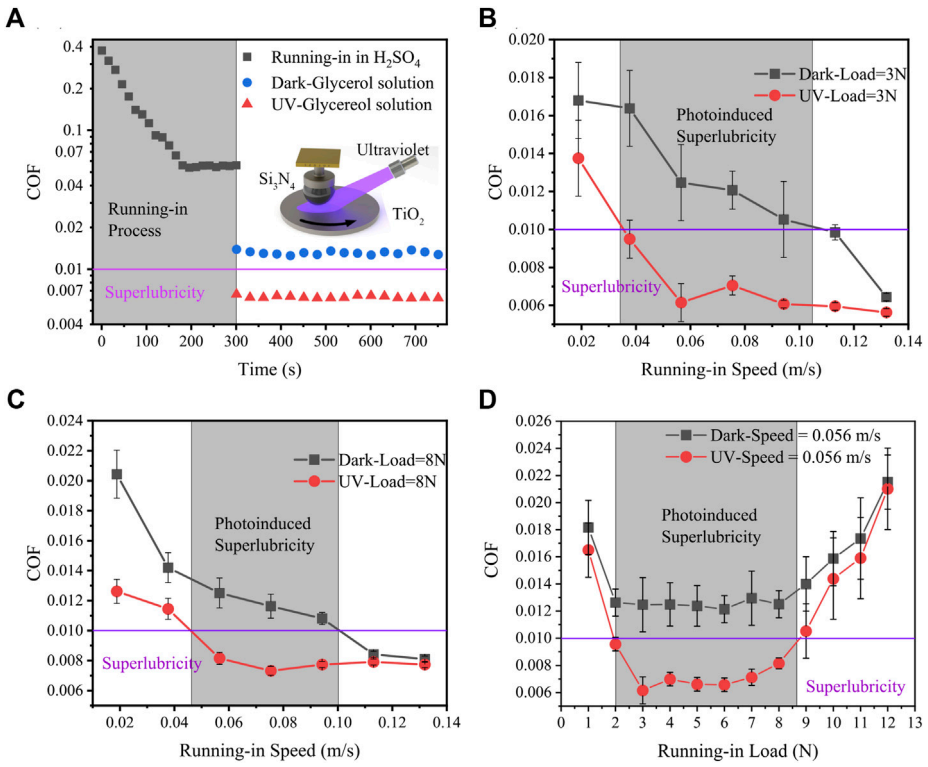

FIGURE 1
(A) Superlubricity was achieved (COF = 0.0062) in 70% glycerol aqueous solution after running-in in H_2SO_4 solution (pH = 1, black square) with ultraviolet illumination (red triangle), while ordinary lubrication was achieved without ultraviolet illumination (blue circle). **(B)** When the load was 3 N, the friction coefficients changed with the increase in the running-in speeds. Photoinduced superlubricity was achieved at a speed from 0.035 m/s to 0.105 m/s. **(C)** When the load was 8 N, photoinduced superlubricity was achieved at a speed from 0.045 m/s to 0.100 m/s. **(D)** When the speed was 0.056 m/s, the friction coefficients changed with the increase in the running-in loads. Photoinduced superlubricity was achieved under a load from 2 N to 8 N.

system reached stability at 0.05. The speed was 0.056 m/s (corresponding to 3 mm radius and 180 revolutions per minute), and the load was 3 N. The 70% glycerol solution showed an outstanding lubrication character, and the friction coefficient reduced to 0.012 after washing out H_2SO_4 solution and adding 5 μl glycerol solution dropwise. In contrast, the UV-treated group had a lower friction coefficient of 0.0062 and entered a superlubricity regime. This phenomenon was called photoinduced superlubricity, as described in our previous work. However, the difference in running-in conditions affected the success of photoinduced superlubricity. Figure 1B demonstrates that when the running-in load was set at 3 N, with the increase in running-in speeds, the friction coefficient of the system decreased and entered a superlubricity regime once the running-in speed was greater than 0.105 m/s. However, ultraviolet illumination reduced the friction coefficient notably, and if the running-in speed was greater than 0.035 m/s, superlubricity would be achieved. Therefore, photoinduced superlubricity was realized when the running-in speeds were set between 0.035 m/s and 0.105 m/s. While the running-in speed was less than 0.035 m/s, both experiment conditions cannot satisfy the requirement of superlubricity, but a decrease in the friction coefficient caused by ultraviolet treatment was still observed. On the other hand, when the running-in speed was greater than 0.105 m/s, superlubricity always existed in the system with or without ultraviolet illumination. As shown in Figure 1C, a similar phenomenon was revealed and the running-in speed section for photoinduced superlubricity shrank to 0.045 m/s from 0.100 m/s when the load increased to 8 N. In Figure 1D, when the running-in speed remained at 0.056 m/s, the friction coefficient decreased with the increase in the running-in load from 1 N to 3 N. However, the friction coefficient reached stability at about 0.013 when the running-in loads were 2–8 N without ultraviolet illumination, and the system entered the superlubricity region when the running-in loads were 3–8 N with ultraviolet illumination. Photoinduced superlubricity failure was achieved when the load was greater than 8 N and with the increase in the running-in load, the difference in the friction coefficient was less obvious before and after ultraviolet illumination.

In addition to the influence caused by different running-in loads and speeds, diverse pH values of sulfuric acid solution affected the photoinduced superlubricity as well. As shown in Figure 2, the friction coefficient showed a rising trend with the increase in pH values in both dark and UV-treated groups in glycerol aqueous solutions after running-in. When the load was 3 N, as shown in Figure 2A, the system was in an ordinary lubrication state without ultraviolet treatment, and when the pH value was 1, the friction coefficient reached the smallest value of 0.0125. UV treatment reduced the friction coefficient significantly, and when the hydrogen ion concentration was higher than 10^{-5}~$10^{-4.5}$ mol/L (pH = 4.5–5), the friction coefficients were less than 0.01 (superlubricity). This result indicated that when the pH values of running-in solutions were less than 4.5–5, photoinduced superlubricity could be achieved in glycerol solution. Similarly, when the load was 8 N, as shown in Figure 2B, the

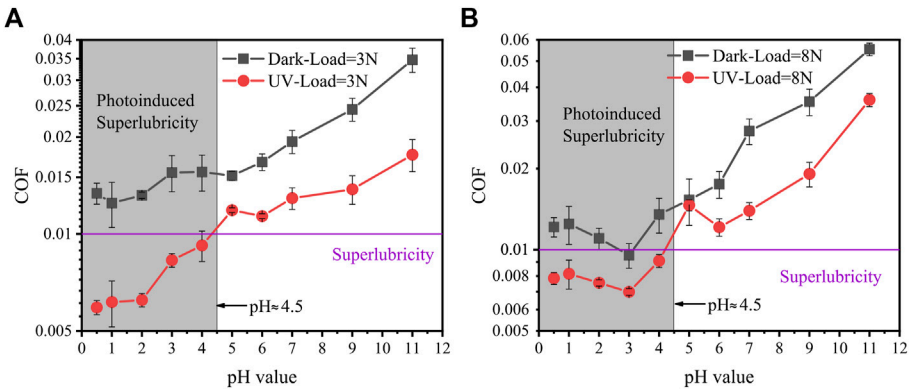

FIGURE 2
Coefficient of friction in 70% glycerol solution changed with the increase in the pH value of sulfuric acid solution after the running-in process under loads of **(A)** 3 N and **(B)** 8 N. After ultraviolet illumination, the red circles were always lower than black squares which were not ultraviolet treated.

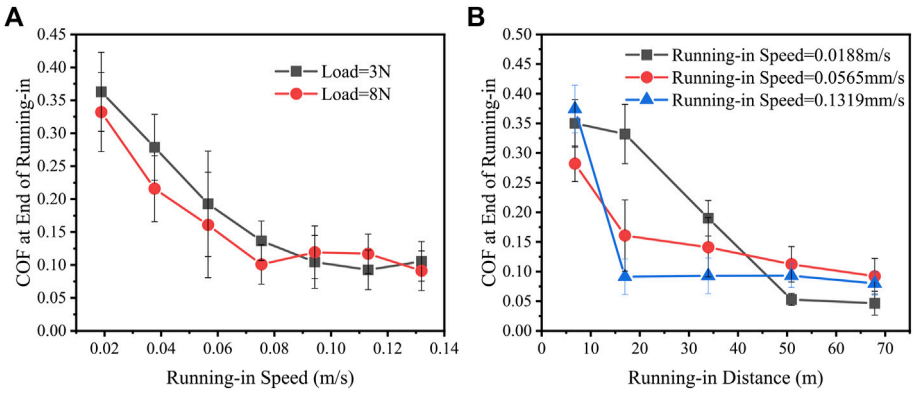

FIGURE 3
(A) In the running-in process, the coefficient of friction (COF) at the end of running-in in H_2SO_4 under loads of 3 N and 8 N decreased with the increase in the running-in speed. The running-in distance was 16.96 m; **(B)** coefficient of friction at the end of running-in under a load of 8 N decreased with the increase in the running-in distance. The running-in speeds were 0.0188 m/s, 0.0565 m/s, and 0.1319 m/s.

smallest friction coefficient value was 0.00954 in acid solution after running-in with a pH value of 3, which was on the boundary line of ordinary lubricity and superlubricity. However, after ultraviolet illumination, the system entered incontestable superlubricity. In addition, Figure 2B shows that the boundary pH value of photoinduced superlubricity was also 4.5–5. Nevertheless, when the pH value of the running-in solution was greater than 5, even turned to be alkaline (pH > 7), the ultraviolet treatment cannot change the ordinary lubrication state to superlubricity, even if the friction coefficient still reduced.

Discussion

The running-in process is believed to create suitable conditions for superlubricity (Li et al., 2014; Deng et al., 2016; Xiao et al., 2017; Han et al., 2019), but what are the suitable conditions for achieving photoinduced superlubricity still remains to be revealed. Figure 3A shows that when the running-in distance was 16.96 m, the friction coefficients at the end of running-in in H_2SO_4 solution differed at different running-in speeds. However, they showed the same trend under the load of 3 N or 8 N. A lower running-in speed, such as 0.018 m/s, would result in a larger friction coefficient (about 0.35 at 0.018 m/s), and when the running-in speed was greater than 0.090 m/s, the coefficient remained stable at about 0.1. Figure 3B shows that when the load was 8 N, with the increase in the running-in distance, the final friction coefficient in H_2SO_4 decreased. When the running-in speed was 0.0188 m/s, the friction coefficient remained stable once the running-in distance was larger than 50 m. When the running-in speed was 0.0565 m/s and 0.1319 m/s, the friction coefficient remained stable when the running-in distance was greater than 16.96 m. The friction coefficient in H_2SO_4 was notably reduced from 0.35 to 0.05 by increasing the running-in speed and time. The trend of the friction coefficient at the end of the running-in process matched with the trend in glycerol solution; therefore, the conditions of the two friction pairs after running-in determined the lubrication state in glycerol and the success of achieving photoinduced superlubricity.

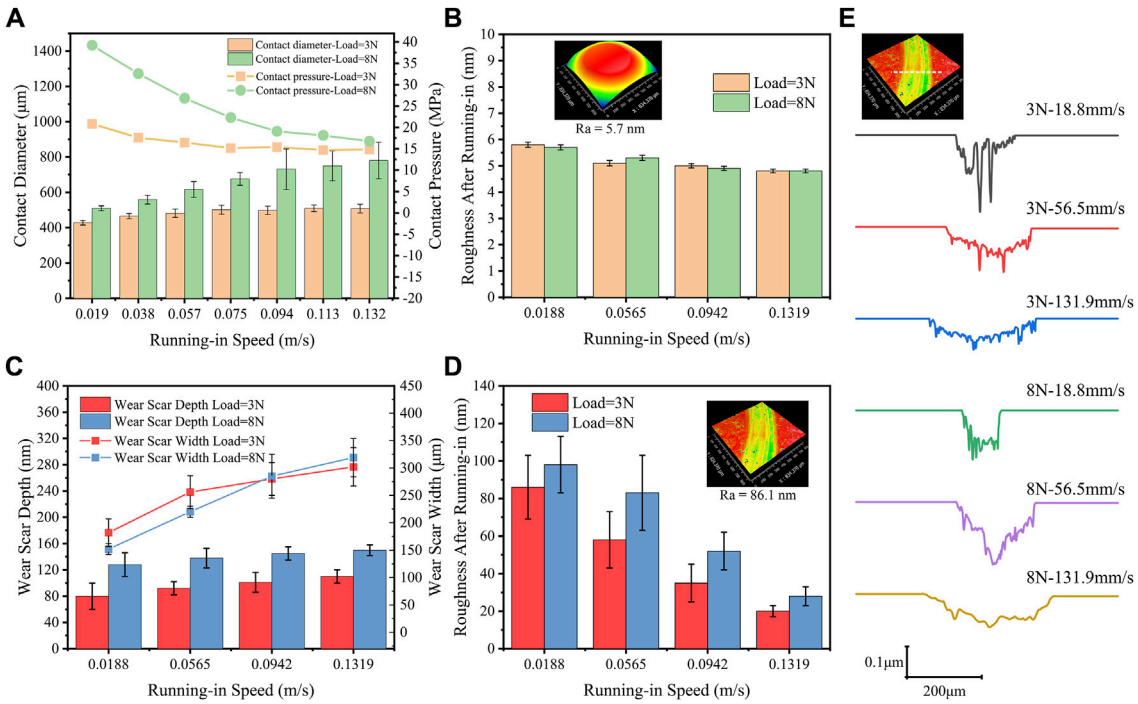

FIGURE 4
(A) Diameters of the wear scar and **(B)** roughness on Si_3N_4 balls under running-in loads of 3 N and 8 N and running-in speed from 0.0188 m/s to 0.1319 m/s (the histogram) and the corresponding calculated contact pressure (the point plot). The running-in distance was 16.96 m. **(C)** Wear scar width and depth and **(D)** roughness of TiO_2 plates after running-in at different running-in speeds and loads. **(E)** Optical image of the wear scar on TiO_2 was on the left top, and the white line represents the cross section of the wear scar. Different cross sections under diverse running-in conditions are shown underneath.

To reveal the secret of the photoinduced superlubricity, the morphology of two surfaces after running-in under different conditions must be studied. Running-in was believed to be a mechanical polishing process for friction pairs, and the wear on the two surfaces created a larger contact area than that calculated by the Hertz contact theory based on point-area contact and dramatically reduced the contact pressure of two friction pairs (Deng et al., 2016). As shown in Figure 4A, after the running-in process, the diameters of the contact area were much larger than the calculated diameters at the beginning of the experiment. Under the load of 3 N and 8 N, the final diameters of wear scars on Si_3N_4 balls were 400–500 μm and 500–700 μm, respectively, which increased with the increase in the running-in speed. As a result, the contact pressure notably decreased, and when the running-in speed was greater than 0.094 m/s, the contact pressure was about 15 MPa. Figure 4C shows that the depths and widths of wear scars on TiO_2 surfaces increased with the increase in running-in speeds. Interestingly, the differences in the depths of wear scars with loads of 3 N and 8 N were more obvious than those in widths of wear scars. This indicated that larger loads during running-in had more influence on plowing the TiO_2 surface. In addition, as shown in Figures 4B, D, the roughness of contact areas on Si_3N_4 balls and TiO_2 plates was measured. With the increase in the running-in speed, the roughness of the wear scar decreased on both surfaces. However, this decrease was more obvious on the TiO_2 surface (from 90 nm to 20 nm) than that on the Si_3N_4 surface (from 5.8 nm to 4.9 nm). Figure 4E shows the cross sections of the wear scar on the TiO_2 plate under different running-in conditions. When the running-in speeds were low (0.018 m/s), sharp peaks or pits appeared on the wear scars, and the width of the scar was narrow. Therefore, the friction coefficients in glycerol solutions after running-in at these low speeds were larger than 0.01 with or without ultraviolet illumination. Superlubricity failure occurred because on such rough surfaces and under high contact pressure, the ratio of dry friction or boundary lubrication was high, so the friction of the system was high. When the running-in speeds were higher (0.056 m/s), sharp peaks and pits were reduced, and the wear scar was broadened. However, peaks and pits still existed and made the system fail in achieving superlubricity. Nevertheless, these asperities provided spots that the glycerol molecules could be adsorbed on. Hence, the direct contact of two solid surfaces was separated by the existence of glycerol molecules after ultraviolet treatment, which resulted in photoinduced superlubricity. When the running-in speeds were high (0.132 m/s), peaks and pits became less, and the wear scars became wider. Lower contact pressure and abrasion of the asperities reduced the direct contact of two friction pairs' surfaces, which meant the ratio of dry friction and boundary lubrication decreased and elastohydrodynamic effect played a more important role. The adsorption of glycerol molecules contributed little to achieving superlubricity in these situations. Therefore, superlubricity was achieved when the running-in speed was high enough with or without ultraviolet treatment.

Figure 5 reveals how the morphology changed when the running-in load changed. As shown in Figure 5A, the wear scar diameters on Si_3N_4 balls and the corresponding contact pressure increased with the increase in running-in loads. However, the wear scar width on TiO_2 plates changed erratically, and the reason might be that the plowing effect was more significant when the load became larger. Similarly, in

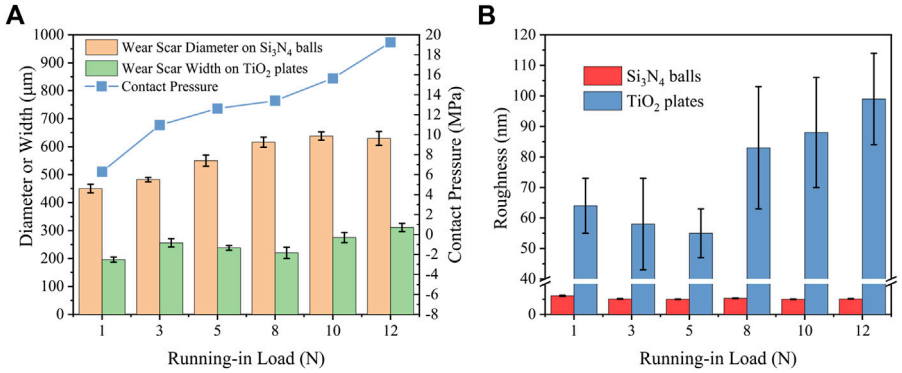

FIGURE 5
When the running-in speed was 0.056 m/s and running-in distance was 16.96 m, **(A)** change in wear scar diameters on Si_3N_4 balls and wear scar width on TiO_2 plates and the corresponding contact pressure with the increase in running-in load; **(B)** roughness change on Si_3N_4 balls and TiO_2 plates with the increase in the running-in load.

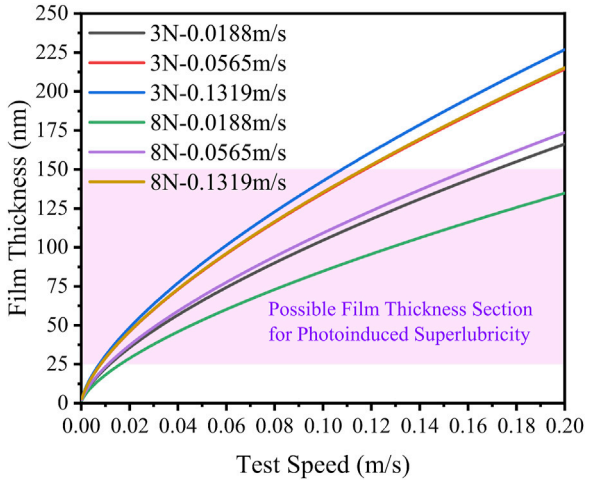

FIGURE 6
Film thickness calculated by the H-D formula in 70% glycerol solution under different running-in conditions. The purple section is possible because of the film thickness section for photoinduced superlubricity because of the lubrication states.

Figure 5B, the roughness on TiO_2 plates decreased to 55 nm and then rose to 99 nm with the increase in the running-in load. However, the roughness on Si_3N_4 showed no apparent difference when the loads changed and remained stable at about 5 nm. The reason for the existence of different morphologies of wear scars on TiO_2 and Si_3N_4 for the same running-in distance might be that different running-in speeds and loads provided different polishing power. Therefore, the total work the outside had contributed to the system differed. The higher the running-in speed was, the more polishing work was performed on the contact area, and the contact area became smoother, leading to a lower friction coefficient, which was similar to the increase in the running-in distance. However, the roughness of the wear scar on Si_3N_4 balls (~5 nm) was much less than that on original Si_3N_4 balls (10 nm), but the roughness of the wear scar on TiO_2 surfaces (20–90 nm) was larger than that on original TiO_2 surfaces (~20 nm). This difference indicated that the polishing mechanism was appropriate for Si_3N_4 surfaces for running-in but not for TiO_2 surfaces, and the mechanism will be discussed later in this chapter.

To further understand the influence of wear scar morphology on the photoinduced superlubricity in the TiO_2/Si_3N_4 tribo-system, the film thickness in glycerol solutions was calculated by the Hamrock–Dowson (H-D) theory as follows:

$$H_c^* = 2.69 \frac{G^{*0.53} u^{*0.67}}{W^{*0.067}} \left(1 - 0.61 e^{-0.73k}\right),$$

where $H_c^* = h_c/R$, $G^* = \alpha E'$, $\mu^* = \eta_0 u/E'R$, and $W^* = W/E'R^2$, where h_c is the film thickness, α is the pressure–viscosity coefficient of the glycerol solution ($\alpha = 6 \times 10^{-9}$ Pa^{-1}), u is the average linear speed of a TiO_2 plate and Si_3N_4 ball, W is the load, k is a coefficient, E′ is the reduced Young's modulus of the two contacting solids, and R is the equivalent radius of the ball that could be described by the Hertz contact theory; in this theory, $R = E'D^3/6W$, where D is the diameter of the worn region of the ball. The calculated results are shown in Figure 6. The lubrication state could be distinguished by using the ratio of the theoretical film thickness to the equivalent surface roughness, and the ratio λ could be calculated by the following formula:

$$\lambda = \frac{h_c}{\sqrt{\sigma_1^2 + \sigma_2^2}},$$

where σ_1 and σ_2 are the surface roughness of the worn regions of the Si_3N_4 balls and TiO_2 plates, respectively. The system was in the elastohydrodynamic lubrication state if the ratio λ exceeded 3, in the mixed lubrication state if the ratio λ was between 1 and 3, and in the boundary lubrication state if the ratio λ was less than 1. According to a previous analysis, the photoinduced superlubricity emerged when there was a proper ratio of the direct contact provided by asperities on the two surfaces. In other words, the lubrication state must be in the mixed lubrication state, and the ratio λ should be between 1 and 3. Combining the theoretical results of the film thickness and the calculated surface roughness, the possible film thickness section for photoinduced superlubricity was marked in Figure 6 with a purple belt. This belt did not represent that every film thickness within the range could make achieving photoinduced superlubricity possible; however, photoinduced superlubricity still depends on the specific

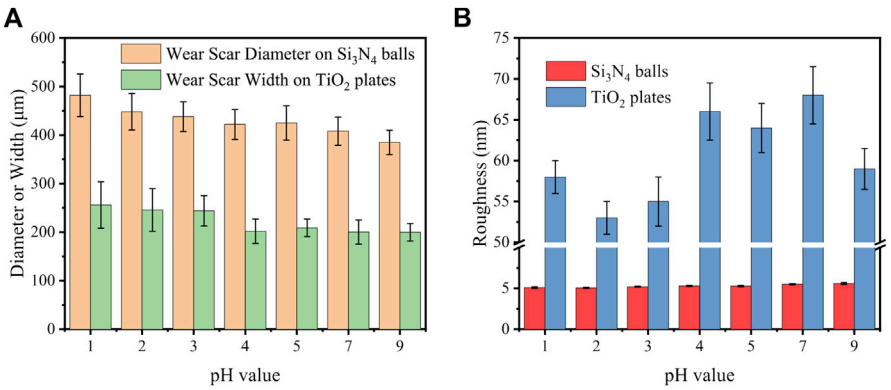

FIGURE 7
(A) Wear scar diameters on Si_3N_4 balls and the wear scar widths on TiO_2 plates and **(B)** roughness on the two friction pairs changed with the increase in the pH value of sulfuric acid solution after the running-in process under a load of 3 N and a speed of 0.056 m/s.

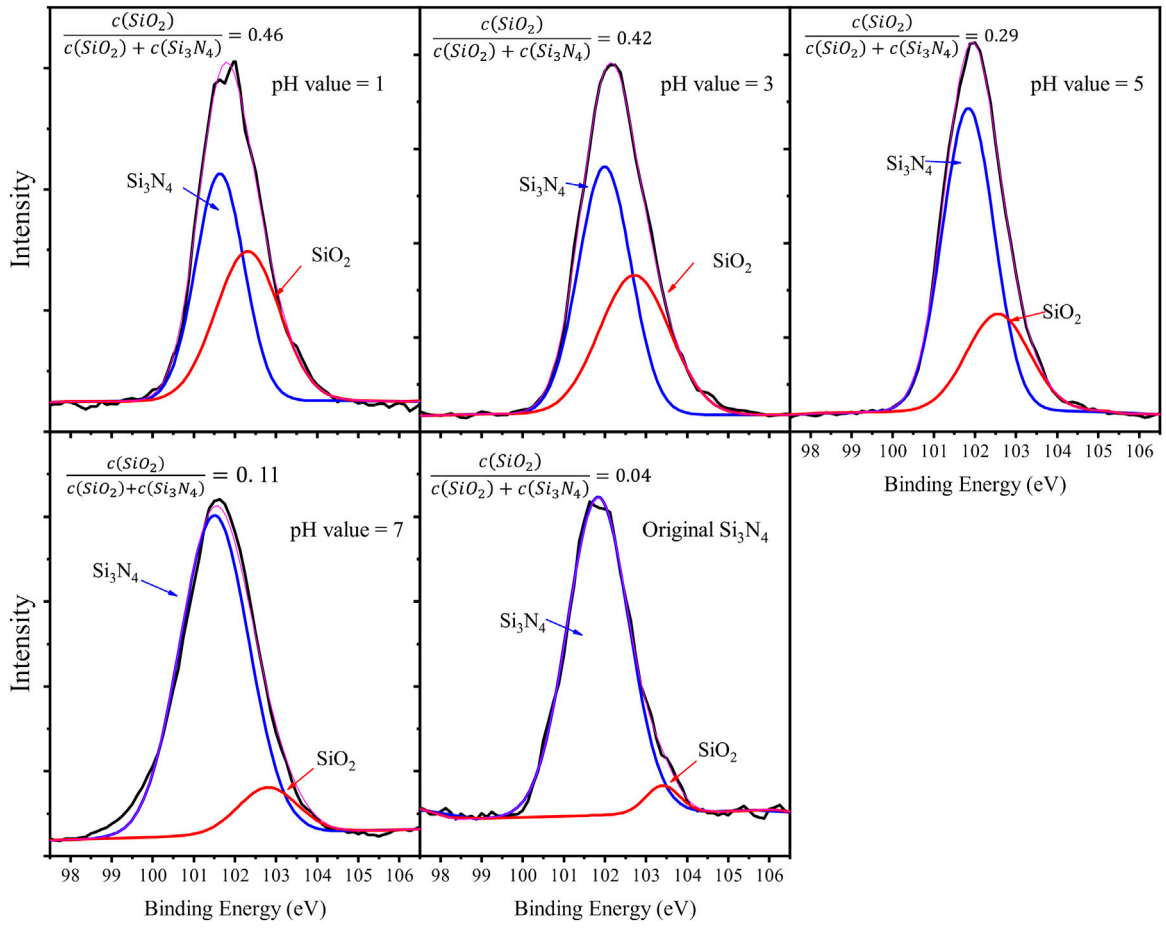

FIGURE 8
XPS results of Si*2p* of wear scars on Si_3N_4 balls (left four images) after running-in in different pH values and the original Si_3N_4 ball (last).

running-in loads and speeds, which determined the morphologies of the wear scars.

The running-in process would not only change the mechanical properties of the surfaces but also provide conditions for chemical reactions on the wear scars. As shown in Figure 7, the wear scar diameters on Si_3N_4 balls and the wear scar widths on TiO_2 plates changed with the increase in pH values of sulfuric acid solution after the running-in process under the load of 3 N and speed of 0.056 m/s. However, this change, as well as the corresponding contact pressure, was not as severe as the friction coefficient change in glycerol

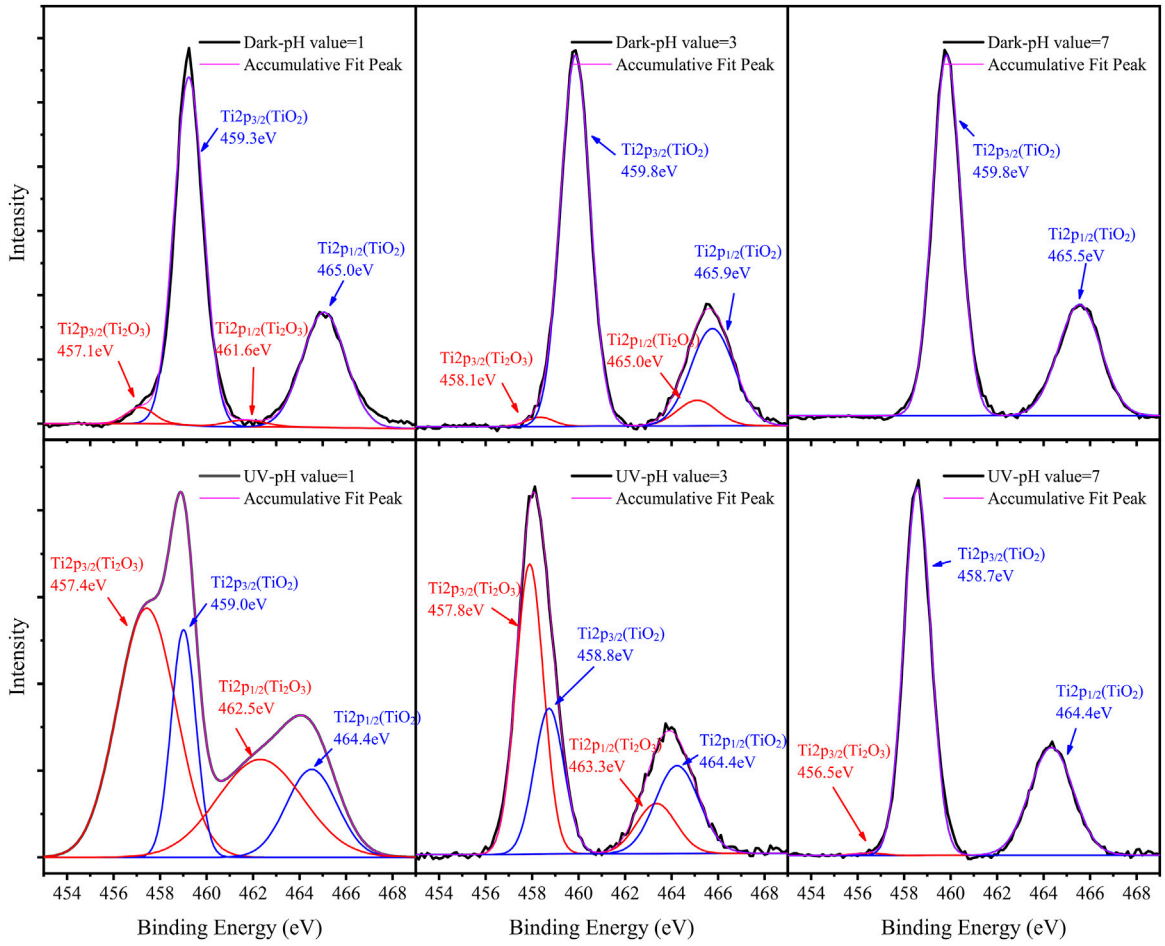

FIGURE 9
XPS results of Ti*2p* of wear scars on TiO_2 surfaces after running-in in different pH values (Hirano and Shinjo, 1990; Dienwiebel et al., 2005; Tian et al., 2022) with and without ultraviolet illumination.

solutions. The morphology change cannot explain the rise of the friction coefficient when the pH value became larger. According to previous studies, a tribochemical reaction occurred in these friction systems during the running-in period. An SiO_2 layer formed through the hydrolysis of silicon nitride in the acid solution on the surface of the Si_3N_4 ball.

$$Si_3N_4 + 6H_2O = 3SiO_2 + 4NH_3 \quad (1)$$

$$SiO_2 + 2H_2O = Si(OH)_4 \quad (2)$$

This reaction results in a reduction in the contact pressure and surface roughness, thereby providing conditions conducive to elastohydrodynamic lubrication. In addition, the appropriate SiO_2 surface on the ball and TiO_2 surface on the plate in the friction test adsorbed hydrogen ions on the surface in the protonation reaction. Hence, the surface became positively charged, and dissolved counter ions, such as SO_4^{2-}, were adsorbed on the surface to balance the surface charge, resulting in the formation of a Stern layer and diffuse double layer. The double layer repulsive force could be produced between two surfaces, and the friction could be reduced. These are the mechanism of a low friction coefficient and even superlubricity in glycerol solution after running-in in acid solution.

Figure 8 displays the XPS spectrums of Si*2p* of wear scars on Si_3N_4 balls. In the last Si*2p* spectrum, the original Si_3N_4 balls' signal consisted of two components whose binding energies were at 102.0 eV and 103.5 eV. The main component at 102.0 eV resulted from silicon in the Si_3N_4 ceramic, while the shoulder at 103.5 eV was associated with silicon in the SiO_2 bond state (Peuckert and Greil, 1987). The relative concentration of SiO_2 on the surface of the original Si_3N_4 ball was 0.04. However, after the running-in process, the relative concentration increased. In deionized water, the concentration was 0.11, and this number increased with the increase in the concentration of hydrogen ions. While the pH values were at 1, 3, and 5, the relative concentrations were 0.46, 0.42, and 0.29, respectively. The concentration increased significantly (from 0.04 to 0.46), however, depending on the pH value of the solution. These results indicated that a silica layer is more easily generated by the running-in process with the acid than by mechanical polishing in water. The existence of the hydrogen ions can accelerate the tribochemical reaction speed. Therefore, pH values of the running-in solution can affect the formation of silica layers on the Si_3N_4 balls. As a result, the friction coefficient was lower when the pH value was lower during running-in. However, this result cannot explain the pH value limits in photoinduced superlubricity because no transformation was observed

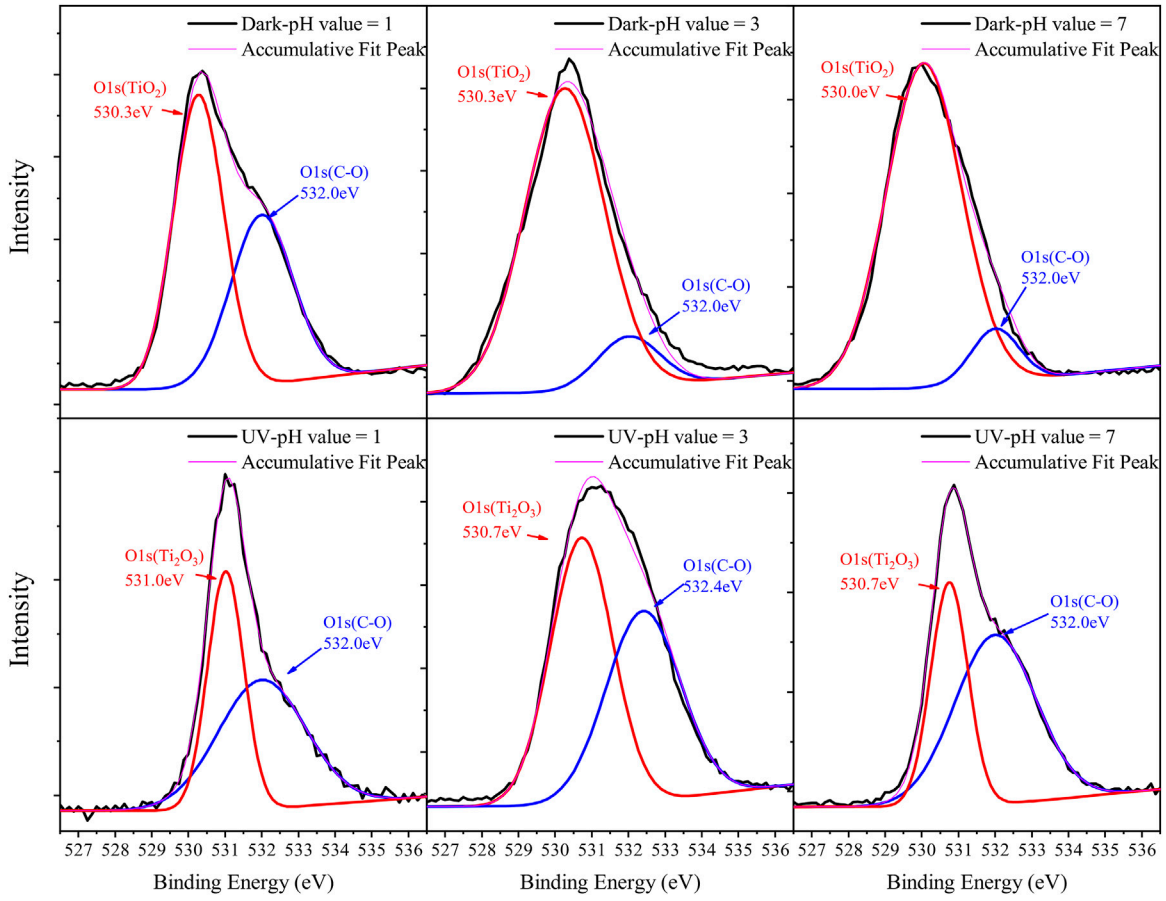

FIGURE 10
XPS results of O*1s* of wear scars on TiO_2 surfaces after running-in in different pH values (Hirano and Shinjo, 1990; Dienwiebel et al., 2005; Tian et al., 2022) with and without ultraviolet illumination.

on Si_3N_4, when the ultraviolet was applied on the surfaces of TiO_2 plates.

As shown in Figure 9, the XPS results of Ti*2p* of wear scars on TiO_2 plates showed different spectrums. Without ultraviolet treatment, the peaks of the Ti*2p* spectrum can be decomposed into two components. For $Ti2p_{3/2}$, the fitting peak that occurred at 457.1 eV–458.1 eV resulted from Ti^{3+} (Ti_2O_3), and the fitting peak that occurred at 459.3 eV–459.8 eV was associated with Ti^{4+} (TiO_2). For $Ti2p_{1/2}$, the fitting peak that occurred at 461.6 eV–463 eV resulted from Ti^{3+} (Ti_2O_3), and the fitting peak that occurred at 464.4 eV–465.9 eV was associated with Ti^{4+} (TiO_2). Polishing in deionized water (pH = 7), the final XPS spectrum revealed that almost no Ti^{3+} from Ti_2O_3 was detected on the wear scars and the surface was covered by Ti^{4+} from TiO_2. However, when the running-in in acid solution (pH = 1, 3), the signal of Ti^{3+} from Ti_2O_3 was captured; however, the fitting peak of Ti^{4+} from TiO_2 was still major. This result indicated that the existence of hydrogen ions in running-in could help the transformation from Ti^{4+} to Ti^{3+}. In Figure 10, the XPS results of O*1s* of wear scars on TiO_2 plates showed that the signal from C–O (532.0 eV) took more of the O*1s* spectrum when pH values decreased without ultraviolet illumination. This indicated that after running-in in acid solution, the glycerol molecules were more likely to adsorb on the surface of TiO_2. Compared with spectrums of Ti*2p*, this enhancement of adsorption was more from Ti^{3+} (Ti_2O_3) by running-in in a solution with more hydrogen ions. In addition, O*1s* spectrums after ultraviolet illumination further verified this conjecture because the signals from C–O (532.0 eV) enhanced and signals from the combination of Ti and O shifted to higher binding energy, which indicated that the large amount of Ti^{4+} changed to Ti^{3+}.

To verify the aforementioned conclusion, the experiments that replaced the upper friction pairs (Si_3N_4 balls) after running-in in acid or water were carried out. The running-in speed was 0.056 m/s, and the load was 3 N. Figure 11A illustrates the three experiments with different friction pairs. In Figure 11B, the Si_3N_4 ball that experienced running-in in deionized water and the TiO_2 plate that experienced running-in in H_2SO_4 (pH = 1) were taken as the friction pairs. However, this system did not show lubricity as good as that had been both running-in in the acid solution or in the deionized water. This phenomenon might attribute to the unmatched morphology on two surfaces and that the rare silica layer was formed on the Si_3N_4 ball. However, after ultraviolet illumination, friction reduction in this system could still be observed, especially when the test speeds were between 0.02 m/s and 0.06 m/s. This reduction in the friction coefficient resulted from the enhancement of glycerol molecule adsorption, but a lack of a proper condition made the system far away from achieving superlubricity. However, in Figure 11C, photoinduced superlubricity could be achieved with the Si_3N_4 ball after running-in in H_2SO_4 solution and the TiO_2 plate after running-in

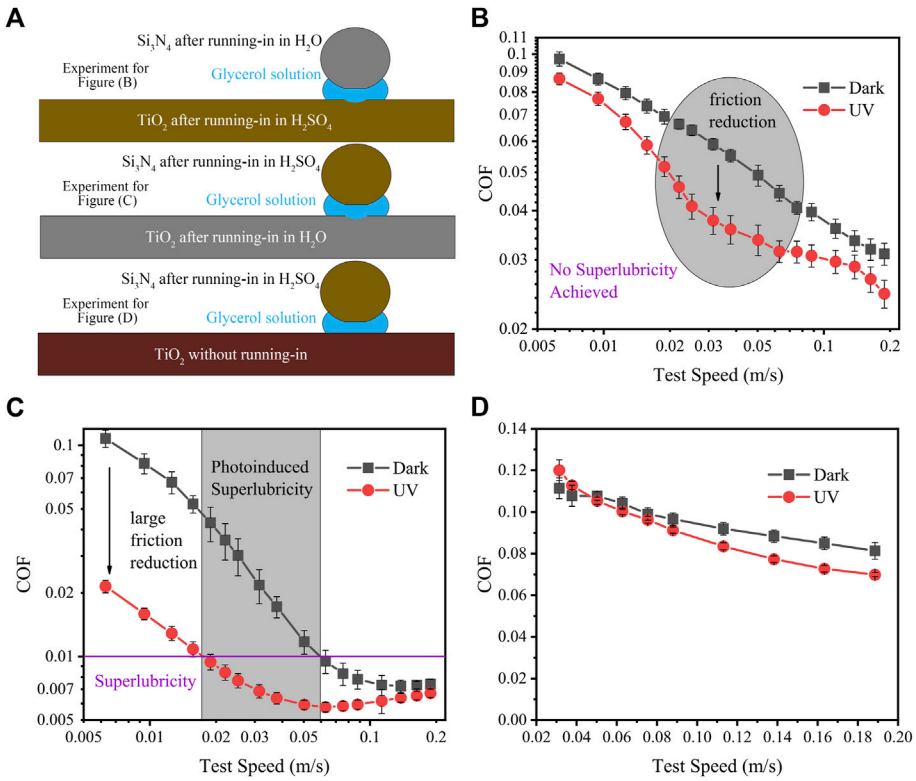

FIGURE 11
(A) Illustrations for the friction test with and without ultraviolet treatment at different test speeds in 70% glycerol solution **(B)** with Si_3N_4 balls after running-in in deionized water and TiO_2 after running-in in H_2SO_4 (pH = 1); **(C)** with Si_3N_4 balls after running-in in H_2SO_4 (pH = 1) and TiO_2 after running-in in deionized water; and **(D)** with Si_3N_4 balls after running-in H_2SO_4 (pH = 1) and TiO_2 without running-in.

in deionized water taken as friction pairs. The test speed range of photoinduced superlubricity lay in the range of 0.02–0.06 m/s which was the same as that in the experiment in Figure 11B. In addition, when the test speed was less than 0.02 m/s, photoinduced superlubricity failed, but a larger friction reduction still existed; when the test speed was higher than 0.06 m/s, superlubricity was achieved without ultraviolet illumination, which even had no obvious effect on the friction coefficient. This result indicated that enhancement of glycerol molecule adsorption caused by ultraviolet illumination worked in the friction system after running-in in both acid solution and water (also shown in Figure 10) and led to friction reduction in boundary lubrication and mixed lubrication. Interestingly, in Figure 11C, the Si_3N_4 ball that experienced running-in in deionized water and untreated TiO_2 plate (with a roughness of 20 nm) were taken as the friction pairs, and the friction coefficients were much higher (0.07–0.12). Ultraviolet treatment did not work in this experiment. These results showed that the roughness of the wear scars on TiO_2 plates was not as important as the electrical property change of Ti atoms. In addition, the running-in provided surfaces that matched with each other so that better lubrication can be achieved. Nevertheless, photoinduced superlubricity relied on not only the enhancement of glycerol molecule adsorption but also other conditions, such as the formation of a silica layer, appropriate test loads and speeds, and well-matched surfaces.

The aforementioned experimental results revealed that the speeds, loads, and pH values of the solution were important for photoinduced superlubricity during running-in. As shown in Figure 12A, appropriate speeds and loads can polish the contact surfaces of Si_3N_4 balls, reduce the contact pressure, and make two friction pairs' surfaces matched to each other, which results in mixed lubrication in 70% glycerol solution. In Figure 12B, high speed or low load smooths the wear scar and further reduces the contact pressure; therefore, when tested in glycerol solution, the major lubrication mechanism was from the elastohydrodynamic effect. Despite the adsorption of glycerol molecules on asperities, the effect on the friction of the whole system was unapparent. In Figure 12C, a low speed or large load makes the wear scar rougher, and when tested in glycerol solution, boundary lubrication and even dry friction between asperities dominate, which increases the friction of the system and breaks the superlubricity. After ultraviolet illumination, adsorption of glycerol molecules can help reduce the shear force between asperities; however, a lack of elastohydrodynamic effect still leads to superlubricity failure. On the other hand, enough hydrogen ions accelerate the hydrolysis on Si_3N_4, and more silica layers are formed in solutions with lower pH values. The silica layer provides lower pressure under the same loads and has low shearing strength, which can help reduce the friction. In addition, the formation of the silica layer smooths the surface of the Si_3N_4 ball and provides a surface for a diffused double layer, which further reduces the friction of the system (Deng et al., 2016). TiO_2 is more likely to adsorb the glycerol molecules after running-in in acid solution with more hydrogen ions because of the reaction between TiO_2 and water molecules. After ultraviolet illumination, adsorption becomes much

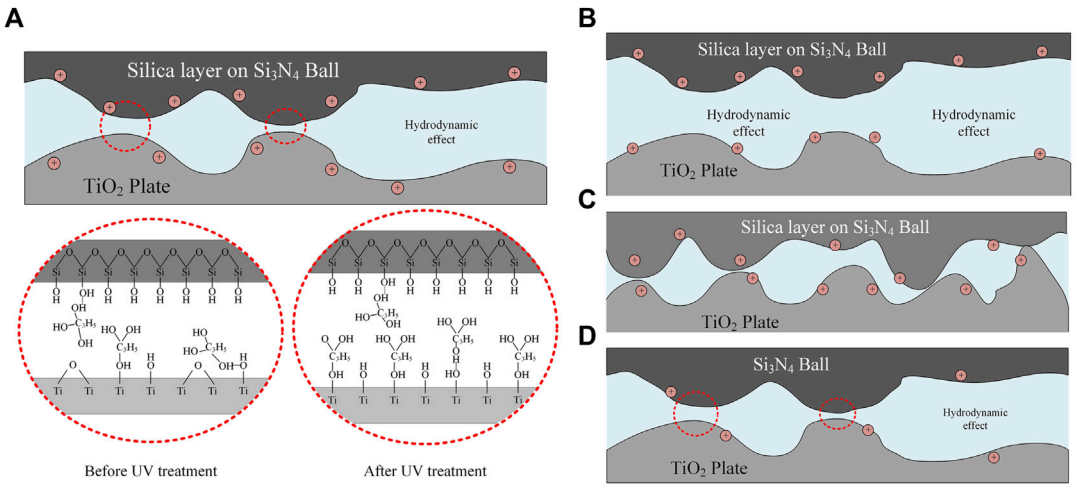

FIGURE 12
(A) Mechanism of photoinduced superlubricity. The failure mechanism of photoinduced superlubricity: **(B)** film thickness was large enough to separate two friction surfaces and the elastohydrodynamic effect dominated; **(C)** film thickness was low and the boundary lubrication dominated; **(D)** silica layer had not been formed and adsorption of hydrogen ions and glycerol molecules was not enough to separate the two friction surfaces.

stronger since a large amount of Ti^{4+} transforms to Ti^{3+} on the TiO_2 surface, and this provides adequate spots for adsorption. The adsorption of glycerol molecules prevents the direct contact of two asperities, leading to the reduction in the shearing force between two surfaces. As shown in Figure 12D, if the system experienced the running-in process in solution without enough hydrogen ions, almost no silica layer could be formed on the Si_3N_4 ball surface. Moreover, fewer hydrogen ions were adsorbed on the surface, and the double-layer effect was weakened. On the TiO_2 surface, the lack of hydrogen ions left the surface with less Ti-OH and adsorption of glycerol molecules.

Conclusion

The influence of the running-in process on photoinduced superlubricity is investigated in this study. The results reveal that when the running-in loads are between 3 N and 8 N, speeds are between 0.04 m/s and 0.100 m/s, and pH values are lower than 4.5, photoinduced superlubricity can be achieved in 70% v/v glycerol aqueous solution in the Si_3N_4/TiO_2 tribo-system. Ultraviolet illumination is believed to change Ti^{4+} to Ti^{3+} on the TiO_2 surface and enhance the adsorption of glycerol molecules during lubrication, and this adsorption can prevent direct contact of two asperities and reduce the shearing force. When the system is in a mixed lubrication state, contribution from this adsorption will help the system achieve superlubricity along with an elastohydrodynamic effect. During running-in, the surface of Si_3N_4 experiences mechanical polishing which makes the surface smoother and the contact pressure lower. In addition, the formation of the silica layer helps further reduce contact pressure and provides an electrical double layer on asperities. Different running-in loads and speeds have similar results, while higher pH values can slow down the formation of the silica layer, which weakens the lubricity of the silica layer. As for TiO_2 plates, during running-in, the plowing effect takes place and the wear scar becomes rougher, but on the other hand, better matched to the wear scar of Si_3N_4. This leads to the mixed lubrication state when replaced by glycerol solution as the lubricant with higher viscosity. In addition, running-in in acid turns Ti^{4+} to Ti^{3+}, which makes the surface more likely to adsorb glycerol molecules on asperities and reduces direct contact of two surfaces after running-in. However, low running-in speeds and loads or too high loads can make the surface too rough to form a liquid film, while high running-in speeds can make the surface smooth again, and the liquid film separates two surfaces too far to show the effect of glycerol molecules.

Data availability statement

The original contributions presented in the study are included in the article/Supplementary Material; further inquiries can be directed to the corresponding author.

Author contributions

KH designed and carried out the experiment, analyzed the mechanism, and wrote the manuscript. PM helped carry out the experiment. LM, YT, and JL helped analyze the mechanism.

Acknowledgments

The authors would like to acknowledge the support of the National Natural Science Foundation of China (51922058).

Conflict of interest

The authors declare that the research was conducted in the absence of any commercial or financial relationships that could be construed as a potential conflict of interest.

Publisher's note

References

Chen, X., Kato, T., and Nosaka, M. (2014). Origin of superlubricity in a-C:H:Si films: A relation to film bonding structure and environmental molecular characteristic. *ACS Appl. Mater. Interfaces* 6 (16), 13389–13405. doi:10.1021/am502416w

de Wijn, A. S., Fasolino, A., Filippov, A. E., and Urbakh, M. (2016). Effects of molecule anchoring and dispersion on nanoscopic friction under electrochemical control. *J. Phys. Condens. Matter* 28 (10), 105001. doi:10.1088/0953-8984/28/10/105001

Deng, M., Li, J., Zhang, C., Ren, J., Zhou, N., and Luo, J. (2016). Investigation of running-in process in water-based lubrication aimed at achieving super-low friction. *Tribol. Int.* 102, 257–264. doi:10.1016/j.triboint.2016.05.023

Dienwiebel, M., Pradeep, N., Verhoeven, G. S., Zandbergen, H. W., and Frenken, J. W. M. (2005). Model experiments of superlubricity of graphite. *Surf. Sci.* 576 (1), 197–211. doi:10.1016/j.susc.2004.12.011

Duan, Y., Liu, Y., Li, J., Feng, S., and Wen, S. (2019). AFM study on superlubricity between Ti6Al4V/polymer surfaces achieved with liposomes. *Biomacromolecules* 20 (4), 1522–1529. doi:10.1021/acs.biomac.8b01683

Erdemir, A., Eryilmaz, O. L., and Fenske, G. (2000). Synthesis of diamondlike carbon films with superlow friction and wear properties. *J. Vac. Sci. Technol. A* 18 (4), 1987–1992. doi:10.1116/1.582459

Erdemir, A., Martin, J-M., SuperlubricityErdemir, A., and Martin, J-M. (Editors) (Amsterdam: Elsevier Science B.V.). 2007 2007/01/01/. xvii-xix p.

Evoy, S., Olkhovets, A., Sekaric, L., Parpia, J. M., Craighead, H. G., and Carr, D. W. (2000). Temperature-dependent internal friction in silicon nanoelectromechanical systems. *Appl. Phys. Lett.* 77 (15), 2397–2399. doi:10.1063/1.1316071

Ge, X., Li, J., Zhang, C., and Luo, J. (2018a). Liquid superlubricity of polyethylene glycol aqueous solution achieved with boric acid additive. *Langmuir* 34 (12), 3578–3587. doi:10.1021/acs.langmuir.7b04113

Ge, X., Li, J., Luo, R., Zhang, C., and Luo, J. (2018b). Macroscale superlubricity enabled by the synergy effect of graphene-oxide nanoflakes and ethanediol. *ACS Appl. Mater. Interfaces* 10 (47), 40863–40870. doi:10.1021/acsami.8b14791

Ge, X., Li, J., Wang, H., Zhang, C., Liu, Y., and Luo, J. (2019). Macroscale superlubricity under extreme pressure enabled by the combination of graphene-oxide nanosheets with ionic liquid. *Carbon* 151, 76–83. doi:10.1016/j.carbon.2019.05.070

Ge, X., Li, J., Zhang, C., Liu, Y., and Luo, J. (2019). Superlubricity and antiwear properties of in situ-formed ionic liquids at ceramic Interfaces induced by tribochemical reactions. *ACS Appl. Mater. Interfaces* 11 (6), 6568–6574. doi:10.1021/acsami.8b21059

Goto, K. (1995). The influence of surface induced voltage on the wear mode of stainless steel. *Wear* 185 (1), 75–81. doi:10.1016/0043-1648(95)06600-4

Han, T., Zhang, C., Chen, X., Li, J., Wang, W., and Luo, J. (2019). Contribution of a tribo-induced silica layer to macroscale superlubricity of hydrated ions. *J. Phys. Chem. C* 123 (33), 20270–20277. doi:10.1021/acs.jpcc.9b03762

Han, T., Zhang, S., and Zhang, C. (2022). Unlocking the secrets behind liquid superlubricity: A state-of-the-art review on phenomena and mechanisms. *Friction* 10 (8), 1137–1165. doi:10.1007/s40544-021-0586-1

Hase, A., and Mishina, H. (2010). Magnetization of friction surfaces and wear particles by tribological processes. *Wear* 268 (1), 185–189. doi:10.1016/j.wear.2009.07.011

Hirano, M., and Shinjo, K. (1990). Atomistic locking and friction. *Phys. Rev. B* 41 (17), 11837–11851. doi:10.1103/physrevb.41.11837

Jia, W., Bai, P., Zhang, W., Ma, L., Meng, Y., and Tian, Y. (2019). On lubrication states after a running-in process in aqueous lubrication. *Langmuir* 35 (48), 15435–15443. doi:10.1021/acs.langmuir.9b01105

Jiang, Y., Xiao, C., Chen, L., Li, J., Zhang, C., Zhou, N., et al. (2021). Temporary or permanent liquid superlubricity failure depending on shear-induced evolution of surface topography. *Tribol. Int.* 161, 107076. doi:10.1016/j.triboint.2021.107076

Jiang, Y., Yue, L., Yan, B., Liu, X., Yang, X., Tai, G., et al. (2014). Electric control of friction on silicon studied by atomic force microscope. *Nano* 10 (03), 1550038. doi:10.1142/s1793292015500381

Li, J., Li, J., and Luo, J. (2018). Superlubricity of graphite sliding against graphene nanoflake under ultrahigh contact pressure. *Adv. Sci.* 5 (11), 1800810. doi:10.1002/advs.201800810

Li, J., Liu, Y., Luo, J., Liu, P., and Zhang, C. (2012). Excellent lubricating behavior of brasenia schreberi mucilage. *Langmuir* 28 (20), 7797–7802. doi:10.1021/la300957v

Li, J., Zhang, C., Deng, M., and Luo, J. (2015a). Investigation of the difference in liquid superlubricity between water- and oil-based lubricants. *RSC Adv.* 5 (78), 63827–63833. doi:10.1039/c5ra10834a

Li, J., Zhang, C., Deng, M., and Luo, J. (2015b). Superlubricity of silicone oil achieved between two surfaces by running-in with acid solution. *RSC Adv.* 5 (39), 30861–30868. doi:10.1039/c5ra00323g

Li, J., Zhang, C., and Luo, J. (2014). Effect of pH on the liquid superlubricity between Si3N4 and glass achieved with phosphoric acid. *RSC Adv.* 4 (86), 45735–45741. doi:10.1039/c4ra04970e

Li, J., Zhang, C., and Luo, J. (2013a). Superlubricity achieved with mixtures of polyhydroxy alcohols and acids. *Langmuir* 29 (17), 5239–5245. doi:10.1021/la400810c

Li, J., Zhang, C., Ma, L., Liu, Y., and Luo, J. (2013b). Superlubricity achieved with mixtures of acids and glycerol. *Langmuir* 29 (1), 271–275. doi:10.1021/la3046115

Li, J., Zhang, C., and Luo, J. (2011). Superlubricity behavior with phosphoric acid–water network induced by rubbing. *Langmuir* 27 (15), 9413–9417. doi:10.1021/la201535x

Linsebigler, A. L., Lu, G., and Yates, J. T., Jr. (1995). Photocatalysis on TiO2 surfaces: Principles, mechanisms, and selected results. *Chem. Rev.* 95 (3), 735–758. doi:10.1021/cr00035a013

Liu, Y., Song, A., Xu, Z., Zong, R., Zhang, J., Yang, W., et al. (2018a). Interlayer friction and superlubricity in single-crystalline contact enabled by two-dimensional flake-wrapped atomic force microscope tips. *ACS Nano* 12 (8), 7638–7646. doi:10.1021/acsnano.7b09083

Liu, C., Friedman, O., Meng, Y., Tian, Y., and Golan, Y. (2018b). CuS nanoparticle additives for enhanced ester lubricant performance. *ACS Appl. Nano Mater.* 1 (12), 7060–7065. doi:10.1021/acsanm.8b01632

Liu, D., and Broer, D. J. (2014). Light controlled friction at a liquid crystal polymer coating with switchable patterning. *Soft Matter* 10 (40), 7952–7958. doi:10.1039/c4sm01249f

Liu, W., Wang, H., Liu, Y., Li, J., Erdemir, A., and Luo, J. (2019). Mechanism of superlubricity conversion with polyalkylene glycol aqueous solutions. *Langmuir* 35 (36), 11784–11790. doi:10.1021/acs.langmuir.9b01857

Liu, Y., and Zhang, H. (2022). Roles of transfer layer and surface adhesion on superlubricity behaviors of diamond-like carbon film depending on rotating and reciprocating motion. *Appl. Surf. Sci.* 604, 154538. doi:10.1016/j.apsusc.2022.154538

Luo, J., Liu, M., and Ma, L. (2021). Origin of friction and the new frictionless technology—superlubricity: Advancements and future outlook. *Nano Energy* 86, 106092. doi:10.1016/j.nanoen.2021.106092

Ma, P., Liu, Y., Sang, X., Tan, J., Ye, S., Ma, L., et al. (2022). Homogeneous interfacial water structure favors realizing a low-friction coefficient state. *J. Colloid Interface Sci.* 626, 324–333. doi:10.1016/j.jcis.2022.06.157

Nakata, K., and Fujishima, A. (2012). TiO2 photocatalysis: Design and applications. *J. Photochem. Photobiol. C Photochem. Rev.* 13 (3), 169–189. doi:10.1016/j.jphotochemrev.2012.06.001

Perotti, B. L., Cammarata, A., Cemin, F., Sales de Mello, S. R., Leidens, L. M., Echeverrigaray, F. G., et al. (2021). Phototribology: Control of friction by light. *ACS Appl. Mater. Interfaces* 13 (36), 43746–43754. doi:10.1021/acsami.1c13054

Peuckert, M., and Greil, P. (1987). Oxygen distribution in silicon nitride powders. *J. Mater. Sci.* 22 (10), 3717–3720. doi:10.1007/bf01161483

Sasaki, M., Xu, Y., and Goto, M. (2017). Control of friction force by light observed by friction force microscopy in a vacuum. *Appl. Phys. Express* 10 (1), 015201. doi:10.7567/apex.10.015201

Schirmeisen, A., Jansen, L., Hölscher, H., and Fuchs, H. (2006). Temperature dependence of point contact friction on silicon. *Appl. Phys. Lett.* 88 (12), 123108. doi:10.1063/1.2187575

Sha, T-D., Pang, H., Fang, L., Liu, H-X., Chen, X-C., Liu, D-M., et al. (2020). Superlubricity between a silicon tip and graphite enabled by the nanolithography-assisted nanoflakes tribo-transfer. *Nanotechnology* 31 (20), 205703. doi:10.1088/1361-6528/ab70cd

Tang, S., Li, S., Ma, L., and Tian, Y. (2022). Photorheological fluids of azobenzene polymers for lubrication regulation. *Friction* 10 (7), 1078–1090. doi:10.1007/s40544-021-0529-x

Tang, S., Xue, D., Guo, J., Ma, L., Tian, Y., and Luo, J. (2020). Macroscale light-controlled lubrication enabled by introducing diarylethene molecules in a nanoconfinement. *Langmuir* 36 (21), 5820–5828. doi:10.1021/acs.langmuir.0c00523

Tian, J., Jin, J., Zhang, C., Xu, J., Qi, W., Yu, Q., et al. (2022). Shear-induced interfacial reconfiguration governing superlubricity of MoS2-Ag film enabled by diamond-like carbon. *Appl. Surf. Sci.* 578, 152068. doi:10.1016/j.apsusc.2021.152068

Vu, C. C., Zhang, S., Urbakh, M., Li, Q., He, Q. C., and Zheng, Q. (2016). Observation of normal-force-independent superlubricity in mesoscopic graphite contacts. *Phys. Rev. B* 94 (8), 081405. doi:10.1103/physrevb.94.081405

Wang, H., and Liu, Y. (2020). Superlubricity achieved with two-dimensional nano-additives to liquid lubricants. *Friction* 8 (6), 1007–1024. doi:10.1007/s40544-020-0410-3

Wang, R., Sakai, N., Fujishima, A., Watanabe, T., and Hashimoto, K. (1999). Studies of surface wettability conversion on TiO2 single-crystal surfaces. *J. Phys. Chem. B* 103 (12), 2188–2194. doi:10.1021/jp983386x

Wang, W., Xie, G., and Luo, J. (2018). Superlubricity of black phosphorus as lubricant additive. *ACS Appl. Mater. Interfaces* 10 (49), 43203–43210. doi:10.1021/acsami.8b14730

Wang, Y., Wang, H., and Yan, F. (2009). Effects of UV irradiation on tribological properties of nano-TiO2 thin films. *Surf. Interface Analysis* 41 (5), 399–404. doi:10.1002/sia.3039

Wu, S., Meng, Z., Tao, X., and Wang, Z. (2022). Superlubricity of molybdenum disulfide subjected to large compressive strains. *Friction* 10 (2), 209–216. doi:10.1007/s40544-020-0418-8

Xiao, C., Li, J., Chen, L., Zhang, C., Zhou, N., Qian, L., et al. (2017). Speed dependence of liquid superlubricity stability with H3PO4 solution. *RSC Adv.* 7 (78), 49337–49343. doi:10.1039/c7ra09217b

Xu, J., and Kato, K. (2000). Formation of tribochemical layer of ceramics sliding in water and its role for low friction. *Wear* 245 (1), 61–75. doi:10.1016/s0043-1648(00)00466-x

Yin, X., Jin, J., Chen, X., Ma, T., and Zhang, C. (2021). A new pathway for superlubricity in a multilayered MoS2–Ag film under cryogenic environment. *Nano Lett.* 21 (24), 10165–10171. doi:10.1021/acs.nanolett.1c02605

Zaidi, H., and Senouci, A. (1999). Influence of magnetic field on surface modification and the friction behavior of sliding couple aluminium/XC 48 steel. *Surf. Coatings Technol.* 120-121, 653–658. doi:10.1016/s0257-8972(99)00425-9